

Failure mode transition in nacre and bone-like materials

Reza Rabiei, Saeen Bekah, Francois Barthelat*

Department of Mechanical Engineering, McGill University, 817 Sherbrooke Street West, Montreal, Que., Canada H3A 2K6

ARTICLE INFO

Article history:

Received 18 December 2009
Received in revised form 26 March 2010
Accepted 14 April 2010
Available online 18 April 2010

Keywords:

Biological materials
Fracture
Nacre
Bone
Micromechanics

ABSTRACT

Mineralized biological materials such as nacre or bone achieve remarkable combinations of stiffness and toughness by way of staggered arrangements of stiff components (nanoscale or microscale fibers or tablets) bonded by softer materials. Under applied stress these components slide on one another, generating inelastic deformations and toughness on the macroscale. This mechanism is prominent in nacre, a remarkable material which is now serving as a model for biomimetic materials. In order to better identify which type of nacre should serve as a biomimetic model, the toughness of nacre from four different mollusk species was determined in this study. Nacre from the pearl oyster was found to be toughest, and for the first time remarkable deformation and fracture patterns were observed using in situ optical and atomic force microscopy. Under stress, stair-like deformation bands deformed at an angle to the loading direction, forming a dense, tree-like network. This marks a clear difference from the now well-documented “columnar” failure mode, in which deformation bands are perpendicular to the loading direction. Analytical and numerical models reveal the conditions for the transition between the columnar and stair failure modes, namely large or random overlap between inclusions and local shear stress generated by inhomogeneities in the material. “Stair” failure promotes spreading of non-linear deformation and energy dissipation, which translates into a greater toughness overall. A similar mechanism may also occur in bone, which has a microstructure which is in many ways similar to sheet nacre.

© 2010 Acta Materialia Inc. Published by Elsevier Ltd. All rights reserved.

1. Introduction

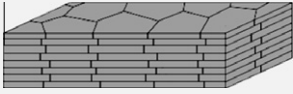
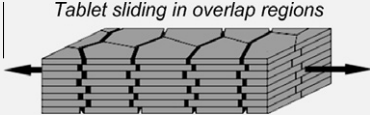
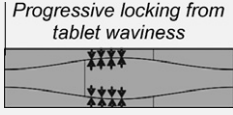
Structural biological materials like seashells or mineralized skeletons are composed of relatively weak, small scale structural components, but assembled in intricate ways that lead to remarkable combinations of stiffness and toughness. In some cases the degree of “amplification” of mechanical performance from the base components is unmatched by any synthetic material [1,2]. A well-known example of this performance is nacre from mollusk shells, which is made of microscopic mineral tablets closely stacked to form a three-dimensional brick wall structure (Table 1). The mineral represents 95 vol.% of the material, the remaining 5 vol.% being organic materials located mostly at the interfaces between tablets [3]. Nacre is therefore a highly mineralized and stiff material, yet it is 3000 times tougher than the brittle mineral it is made of [1]. There is, therefore, a great interest in understanding the mechanisms behind this remarkable performance, in order to duplicate them in artificial, biomimetic materials [2]. In fact, biomimetic materials inspired by nacre have already started to emerge [4,5]. The staggered arrangement of the tablets in nacre dictates a specific mechanism, where applied tensile loads are transferred through tensile stress in the mineral tablets and shear

stress at the softer interfaces between tablets. With sufficient applied load the tablets “slide” on one another, this “sliding” being mediated by thin layers of softer organic materials capable of accumulating large deformations while dissipating energy [6]. Resistance to shearing at the interface is provided by the organic material [6,7], by nanoasperities [8] and by mineral bridges [9]. The tablets also show some waviness, which impedes tablet sliding and generates strain hardening [10], delaying localization and propagating the sliding mechanism over large volumes (Table 1). These mechanisms are now well documented for the case of columnar nacre [10] (columnar nacre from red abalone is perhaps the most studied nacre). In columnar nacre the tablets are arranged in columns (Table 1), with well-defined core and overlap regions [10]. In this quasi-periodic structure sliding only occurs in the overlap regions, generating deformation bands perpendicular to the loading direction [8,10]. Cracks eventually also follow the overlap regions [11].

In contrast, sheet nacre has a more random staggered arrangement, with no well-defined overlap and core regions (Table 1). While tablet sliding has been observed in sheet nacre [3,8,12], its exact deformation and cracking patterns are unclear. In terms of macroscopic properties, previous studies showed that sheet nacre from the pearl oyster *Pinctada margaritifera* is slightly stiffer and stronger than columnar naces [3,8], but this is not true for all sheet naces [3]. It is also not clear which of the two types of nacre

* Corresponding author. Tel.: +1 514 398 6318; fax: +1 514 398 7365.
E-mail address: francois.barthelat@mcgill.ca (F. Barthelat).

Table 1
Tablet arrangements for columnar and sheet nacles with known deformation and hardening mechanisms.

Microstructure	Deformation mechanism	Hardening mechanism
<p><i>Columnar</i></p> 	 <p>Tablet sliding in overlap regions</p>	 <p>Progressive locking from tablet waviness</p>
<p><i>Sheet</i></p> 	<p>Tablet sliding, but deformation pattern unclear</p>	<p>Not known</p>

tends to be toughest. This is a lack in the context of biomimetic materials, because fabrication procedures have now been refined to a degree allowing unprecedented control over the microstructure [4,13]. Identifying the best natural nacre to serve as a “biomimetic model material” has therefore become increasingly important.

Nacre is part of a wider category of mineralized tissues with a “staggered arrangement” of stiff inclusions aligned along the direction of loading and bonded by softer organic materials. Bone, for example, also follows this “universal” microstructural design over multiple length scales [14]. In particular, the sliding of mineralized collagen fibrils along one another on the microscale was demonstrated to provide the large inelastic strains observed on the macroscale [15]. There are several analogies between nacre and bone, but the experimental study of the failure of bone at small length scales is considerably more difficult than that of nacre, because of the helicoid lamellar structure of the osteons [18]. In terms of modeling, small two-dimensional representative volume elements are typically used [16,17] so as to capture the load transfer from shear at the interface to tension in the inclusions. These models provide analytical solutions for modulus and strength and useful insights into micromechanical design and structural optimization. This type of model, however, relies on the assumption that the structure and displacement are periodic. In consequence, the models predict that the separation of the inclusions forms a uniform network of deformation bands perpendicular to the loading direction. In reality it may not be the case because mineralized fibrils follow a random overlap, so that the failure of bone on those length scales may follow the “stair” pattern described here.

In this article a comparative study of the fracture toughness of four selected nacles is first presented. Significant differences in toughness are reported and, in addition, a new “stair” type of failure mode was observed in sheet nacre. In the second section a simple analytical model demonstrates how the transition between “stair” and “columnar” failure modes is controlled by a combination of microstructure and local shear stress. This finding is finally confirmed by larger scale numerical simulations presented in the last section. The implications on biomimetics and on our understanding of how natural composites with staggered arrangements deform and fail is finally discussed.

2. The fracture of sheet and columnar nacles

The nacles tested in this study consist of two columnar nacles and two sheet nacles. Besides different tablet arrangements, the tablets themselves showed a range of thicknesses and aspect ratios (Table 2). Top shell showed the thickest tablets, followed by pearl oyster, red abalone and pen shell. The tablet aspect ratio was high-

Table 2

Characteristics of the nacles tested in this study (thickness and aspect ratio given as means \pm standard deviation).

Species	Nacre type	Tablet thickness (μm)	Tablet aspect ratio
Top shell (TS) <i>Trochus niloticus</i>	Columnar	0.74 ± 0.08	10.80 ± 3.47
Red abalone (RA) <i>Haliotis rufescens</i>	Columnar	0.45 ± 0.06	12.49 ± 7.97
Pearl oyster (PO) <i>Pinctada margaritifera</i>	Sheet	0.50 ± 0.11	8.91 ± 4.68
Pen shell (PS) <i>Pinna nobilis</i>	Sheet	0.43 ± 0.10	14.37 ± 9.04

est in pen shell, followed by red abalone, top shell and pearl oyster, which displayed the tablets with the smallest aspect ratio. These differences in mean thicknesses and aspect ratios between each of the four species were highly statistically significant ($P < 0.001$ from an independent sample t -test with $n = 250$).

2.1. Specimen preparation

Specimens were prepared by first harvesting a 20×50 mm plate from the shells using a diamond saw. The surfaces of the plate were then ground and finished using a milling machine in order to obtain flat and parallel faces. The plate was then cut into slices using a high precision diamond saw. At this point a pre-notch was made using a diamond saw. One side of the specimen was then polished and the notch was deepened and sharpened with a fresh razor blade. The specimens were oriented so cracking would occur across the layers (Fig. 1). Typical specimen dimensions were 20 mm long, ~ 0.1 –1 mm thick and ~ 0.2 –2 mm wide. Moreover, in order to comply with the ASTM requirement [18], the notch length was maintained within ~ 0.45 – 0.55 of the width. Samples were kept hydrated throughout all the steps of preparation, storage and experiment.

2.2. Experimental procedure

The fracture tests were performed using a four point bending fixture mounted on a miniature loading stage (Ernest F. Fullam Inc., Latham, NY). Four point bending was preferred over three point bending because it generates a more uniform bending moment, enabling potential deflection of the crack away from the initial crack line. The loading stage and sample were first placed under an optical microscope (BX-51M, Olympus, Markham, Canada) equipped with a CCD camera (RETIGA 2000R, Qimaging, Surrey, Canada) and the specimens were loaded at a rate of 0.002 mm s^{-1} up to failure.

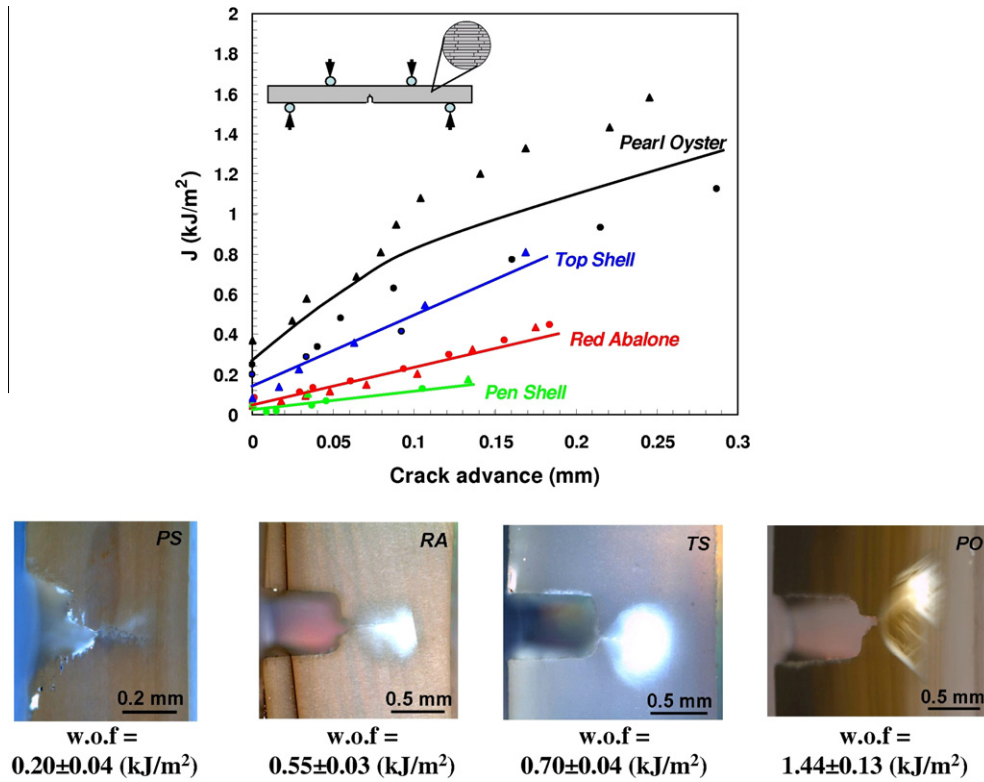


Fig. 1. Fracture resistance curves for four nacles and optical images obtained in situ (in order of increasing toughness). The work of fracture (w.o.f.) for each nacre is also given.

2.3. Fracture tests results

In order to compute the fracture resistance curves, the crack length was measured from the optical images taken during the experiment. The specimens developed large inelastic regions around the crack, such that the linear elasticity-based K_{IC} toughness was not deemed appropriate. Instead, a non-linear J inte-

gral-based approach was used following existing testing standards [18]. A data cut-off condition was applied to all curves to ensure the validity of J over the crack extensions [19].

Fig. 1 shows the fracture resistance curves obtained. Upon crack propagation the toughness increased with crack advance, which is consistent with the stable crack propagation observed during the experiments. A raising crack resistance curve is an indication of

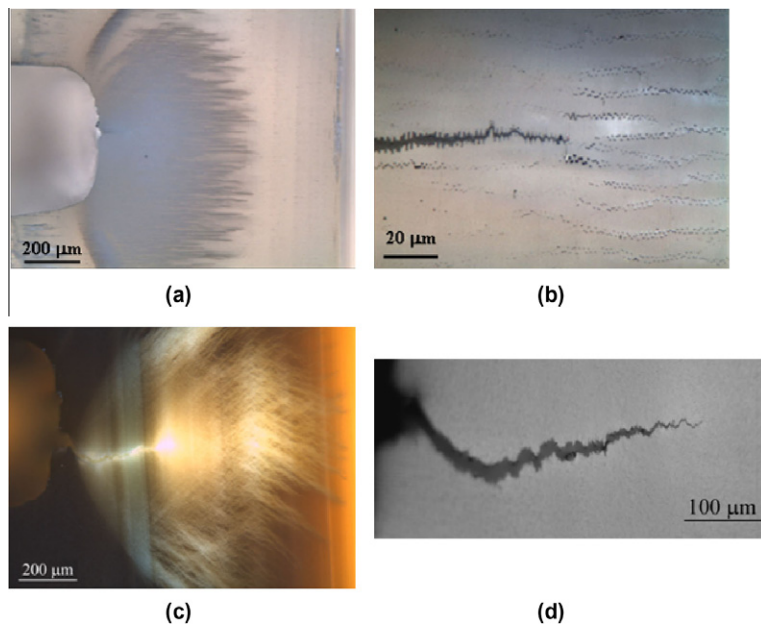


Fig. 2. Optical images from fracture tests. (a) Top shell shows a relatively homogeneous inelastic region and (b) a straight crack which follows tablet columns (note recovery behind the crack tip). (c) Pearl oyster develops a network of localized inelastic branches at an angle and (d) the crack advances in a jagged manner.

toughening mechanisms operating around the advancing crack. The amount of toughening was, however, different across species. The pearl oyster showed the most pronounced toughening, while the pen shell showed only a modest increase. The pearl oyster also displayed the most complex crack patterns (Fig. 2d), which complicated crack length measurements. For all species the crack advance in Fig. 1 was defined as the projected length of the crack along the initial crack line. The variation of crack path across pearl oyster specimens can probably explain the greater variations in the crack resistance curve compared with the other species. The data reduction also relied on assumptions typically made for metals [18], which may be questionable for a material like nacre. Therefore, another measure of toughness which does not rely on any assumption of material behavior was also used. The work of fracture, defined as the area under the load–deflection curve divided by the initial surface area of the ligament [20], was computed for each experiment (Fig. 1). The work of fracture was remarkably consistent across all specimens within each species, and the values were in the same range as the toughness measured on the crack resistance curves.

Optical imaging revealed that all nacles developed a white “process zone” ahead of the crack. Stress whitening, now a well-documented phenomenon in nacre [3,8,11], is an indication of tablets sliding (organic ligaments are exposed at the ends of the separated tablets). As the load increased the size of the process zone increased until the crack propagated, activating “virgin” material ahead of the crack tip. Upon crack propagation a wake of inelastically deformed material was observed behind the crack tip. The material in the wake was not as “white” as ahead of the crack, but nevertheless whiter than the surrounding “virgin” material, indicating some strain recovery in the wake. While all species showed a process zone upon fracture, the size and shape of the process zones varied significantly (Fig. 1). The width of the process zone was only about 0.05 mm for pen shell to about 0.5 mm for top shell and red abalone, to up to 1 mm for pearl oyster. Interestingly, the size of the process zone correlates well with the toughness, which confirms that process zone energy dissipation is a prominent source of toughness in nacre [10,11].

The shape of the process zone also varied significantly. For the top shell and red abalone it was roughly round. In red abalone the presence of weaker planes within the material, called growth lines [21], seemed to have constrained the inelastic region in the same way that plasticity is confined in multilayered materials. No growth line was observed in the top shell. The inelastic zone in the pen shell was small and irregular and its shape could not be defined. The most surprising phenomenon occurred in the case of the pearl oyster, in which two distinct branches of localized inelastic deformation emanated initially from the crack tip at about a 60° angle (Fig. 1). As the load increased the crack propagated obliquely within one of the two branches, except for one sample in which the crack propagated along the initial notch orientation.

Upon crack propagation additional sub-branches developed from the main crack, forming a tree-like network of deformation bands. Note that a small amount of branching was previously reported in sheet nacre [8], but not to the extent observed here. Optical images at higher magnification revealed more details of the structure of the process zone in the top shell and pearl oyster (Fig. 2). The whitening distribution was relatively uniform in the top shell, with some distinct deformation bands perpendicular to the loading direction on the front side of the process zone. The crack propagated in a relatively straight path along individual columns, remaining in an overlap region (the crack is deflected by a few microns at most, Fig. 2b). In contrast, the process zone in the pearl oyster consisted of a network of deformation bands at about a 45° angle from the loading direction (Fig. 2c). This network was denser near the crack tip, but remained inhomogeneous. Crack

deflection was significant, with deflections exceeding 10 μm (Fig. 2d).

In order to elucidate the exact micromechanisms behind the shape of the process zone additional fracture tests were performed on pearl oyster and top shell nacre, but this time under atomic force microscopy (AFM) (Veeco Dimension V, Santa Barbara, CA). The surfaces of the samples were polished down to 0.05 μm following standard polishing procedures, and the samples were kept hydrated throughout the tests. In situ imaging confirmed that for columnar nacre under tensile load all the tablets separate in a homogeneous fashion (Fig. 3a and b). Typical tablet separations were 100 nm, which can account for the 1% tensile strain measured in the tensile tests [11].

Similar images were also acquired in situ for pearl oyster (Fig. 3c and d). The AFM images indicate that tablet sliding was the only inelastic mechanism taking place ahead of the crack tip. This mechanism, however, appeared to be inhomogeneous, with tablets separating in some areas (i.e. area I in Fig. 3) while remaining closed in others (i.e. area II). The separation of the tablets was typically ~ 250 nm (Fig. 3d), more than twice the separation distance observed in the top shell. Fig. 4 shows an AFM image taken just ahead of a crack in sheet nacre. Some junctions remained closed and some areas showed deformation bands at an angle from the loading direction.

This marks a clear difference between columnar and sheet nacles: while columnar nacre fails along all the overlap regions in a “columnar” type of failure, in sheet nacre a “stair” type of failure seems to prevail, leaving some tablet junctions closed. The

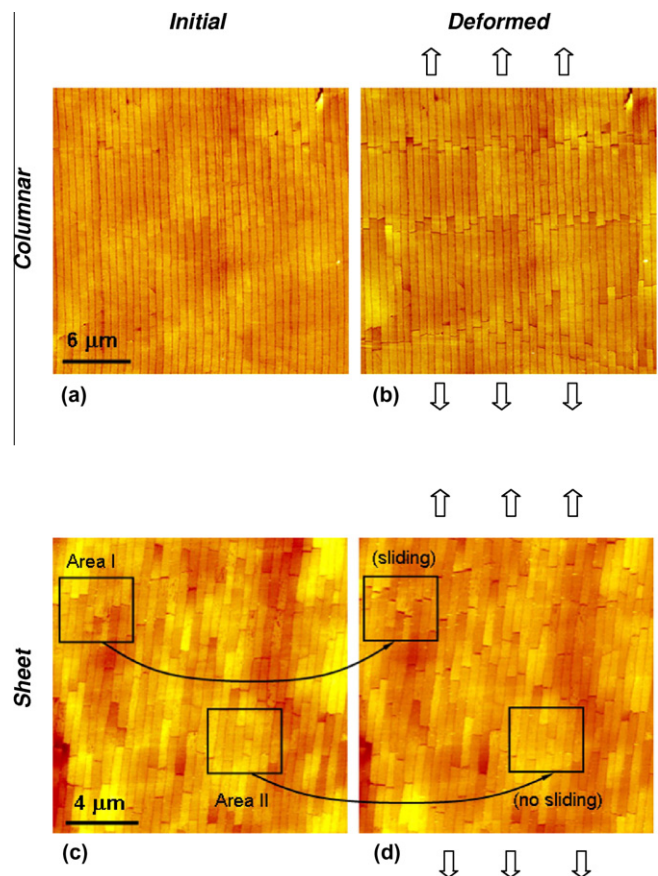


Fig. 3. In situ AFM imaging ahead of a propagating crack. Top shell (a) before and (b) after deformation, showing that all the junctions open, conveying a uniform type of tablet sliding. Pearl oyster (c) before and (d) after deformation, showing that the junctions only opened in some areas while they remained closed in others.

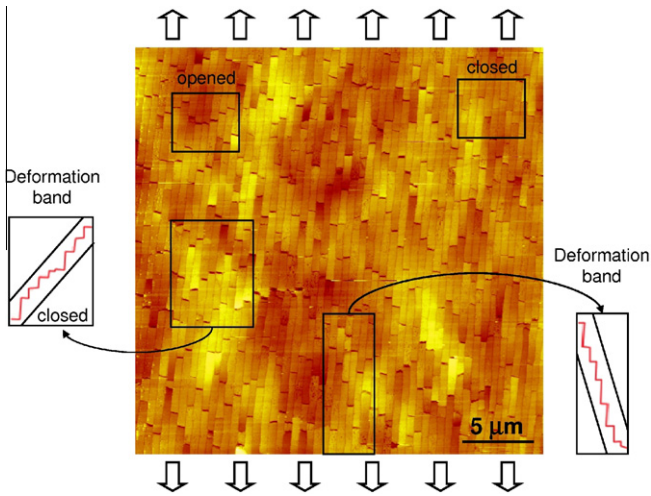


Fig. 4. AFM image of a sheet nacre fracture sample just ahead of a crack. Some junctions remain closed while others are open. Some areas show evidence of deformation bands at an angle from the loading direction.

micromechanisms behind these different failure modes are explored in the next section.

3. Analytical model

In order to capture the differences in mechanism between columnar and sheet nacles a representative volume element

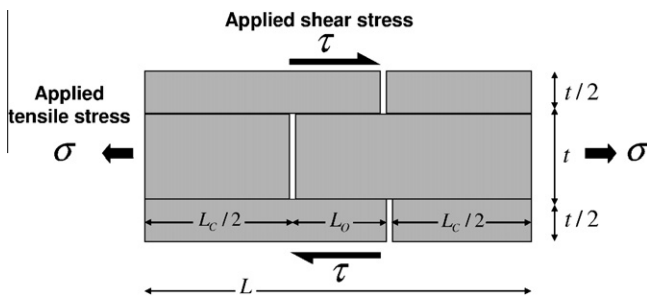


Fig. 5. Representative volume element with dimensions. L, tablet length; t, tablet thickness; L₀, tablet overlap length; L_c, tablet core length.

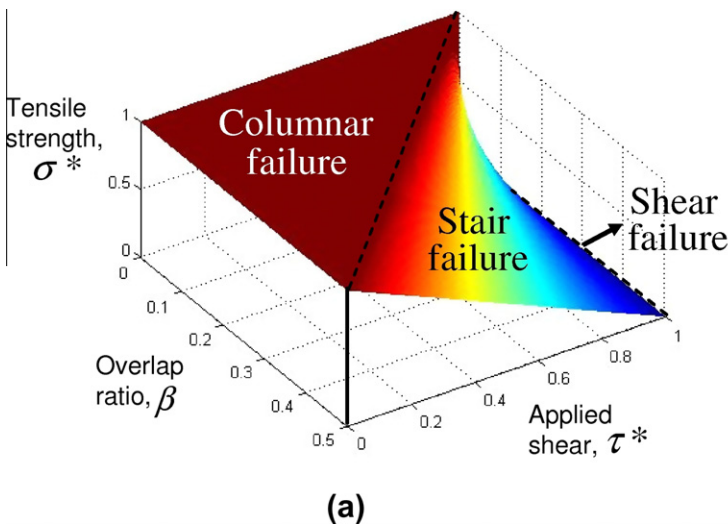


Fig. 6. (a) RVE failure map for different combinations of applied stresses and RVE geometry. (b) Shear stresses around a crack in mode I and associated potential stair failure patterns.

Table 3 Possible RVE failure modes with their conditions and their associated tensile strengths.

Condition	Failure mode	Tensile strength
$0 < \tau^* < 1 - 2\beta$	“Columnar” 	$\sigma = \alpha\tau_s$
$1 - 2\beta < \tau^* < 1$	“Stair” 	$\sigma = \frac{\alpha}{2\beta}(\tau_s - \tau)$
$\tau^* = 1$	“Shearing” 	N/A

(RVE)-based analytical model was developed. Fig. 5 shows the RVE built for a nacreous structure where tablets of length L and thickness t have a constant overlap length L₀ and core length L_c [10]. The RVE was subjected to external tensile and shear stresses resembling the condition the tablets experienced around the crack. The shear strength of the interface is designated τ_s throughout the model.

Table 3 summarizes the main results of this model (calculation details are provided in Appendix A). In essence, the difference in failure mode between columnar and sheet nacre can be explained by the microstructure and by local shear stresses. In particular, if the applied shear stress is sufficiently large and the core region is sufficiently small, the deformation path will follow a “stair” pattern. The transition between columnar and stair failure modes is therefore controlled by a combination of the applied non-dimensional shear $\tau^* = \tau/\tau_s$ and by the microstructure through the overlap ratio $\beta = L_0/L$ (Table 3). The RVE tensile strength was also calculated for each of these failure modes (as a function of tablet aspect ratio $\alpha = L_0/t$). Stair failure was found to lower the tensile strength of the material. Finally, a third type of failure is possible if the applied shear reaches the shear strength of the interface, τ_s . In this case a “shearing” type of failure prevails (Table 3).

Another way to visualize the failure mode transition is through a failure map function of overlap ratio β and applied shear stress τ^* (Fig. 6a). These results show that a nacre with small overlaps (as in columnar nacre) is more likely to fail by columnar failure, while large overlaps (as in sheet nacre) more likely lead to a “stair” failure mode (which is in agreement with the experimental observations).

Stair failure is triggered by local shear stresses, which may be generated by the inhomogeneity of the material: any softer region in a material in tension will generate shear stresses locally. For example, a crack loaded in mode I will develop local shear stresses

that may trigger stair failure (Fig. 6b). Any other softer region in the microstructure will generate similar local shear stress patterns.

4. Numerical model

The transition between columnar and stair failure modes was also captured by numerical models. Large plane strain finite elements models of nacre microstructures were generated, with periodic geometries in both the longitudinal (x) and transverse (y) directions. Each tablet was modeled as linear elastic ($E = 100$ GPa

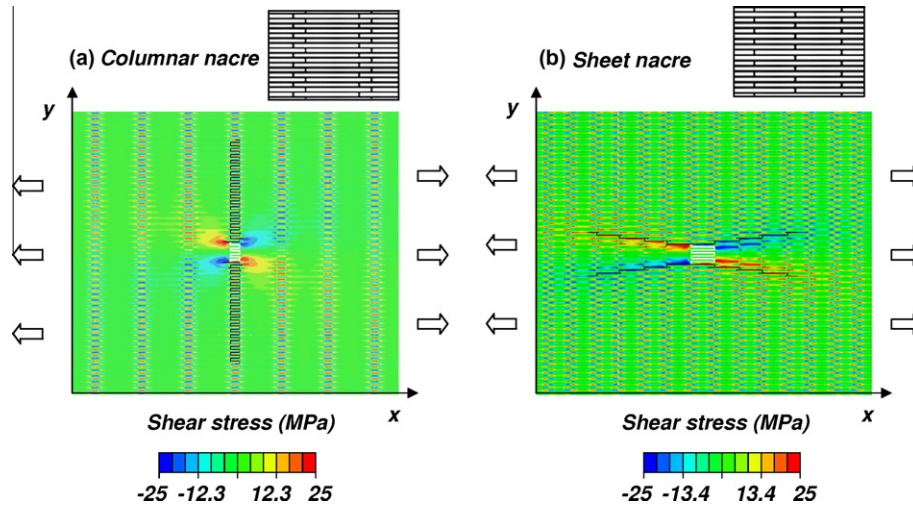


Fig. 7. Shear stress contours for RVE of (a) columnar and (b) sheet nacles. The initial defect is outlined in white. The interfaces that have completely failed are highlighted in black. (Note that tablets orientation and loading direction are rotated by 90° compared with Fig. 2).

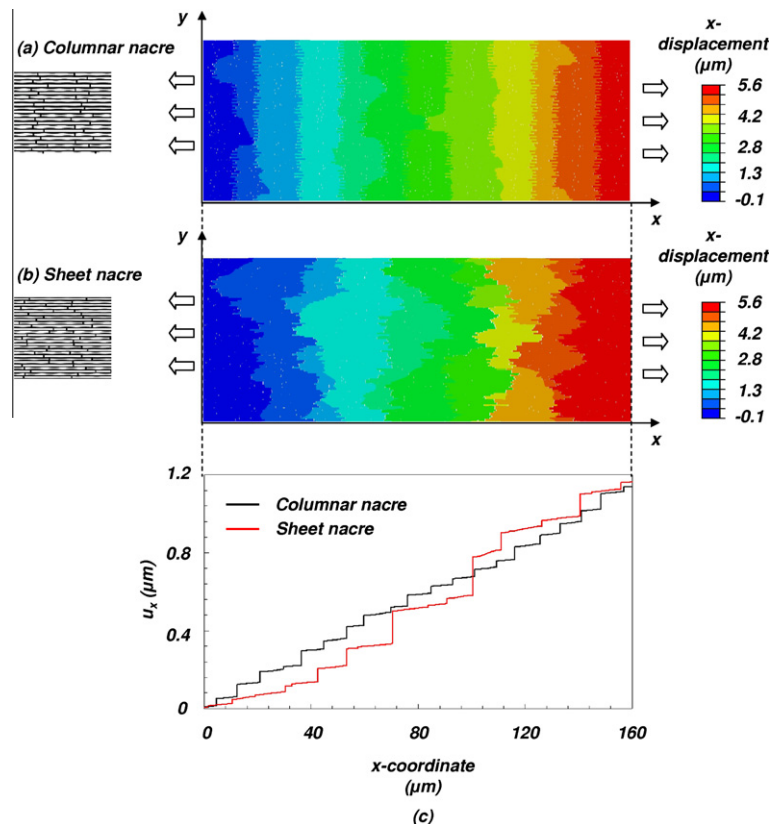


Fig. 8. Contours of the horizontal displacements u_x (along the loading direction) for (a) columnar and (b) sheet models. (c) Displacements u_x along the lower boundary of the models showing different failure patterns (each step on this plot corresponds to a pair of tablets separating). All data plotted at 0.35% macroscopic strain.

[22,23]) with linear plane strain elements, while the interfaces were modeled by inserting cohesive elements between the tablets. The associated cohesive law was taken as described in Barthelat et al. [10]: a short linear elastic region was followed by a long plateau at constant strength ($\tau_s = 25$ MPa). For all models a stretch was imposed along the longitudinal (x) direction. Simulations were performed using ABAQUS (v. 6.8-3, ABAQUS Inc., Providence, RI).

4.1. Periodic structures

At first two large RVEs were generated to perfectly model periodic columnar and sheet microstructures. Both models were composed of tablets $0.5 \mu\text{m}$ in thickness and $5 \mu\text{m}$ in length. In columnar nacre the overlap was set at 20% of the length of the tablets ($\beta = 0.2$, Fig. 7), while in sheet nacre the overlap was set to 50% of the length of the tablets ($\beta = 0.5$). In both models a defect was introduced in the center of the RVE by removing a few cohesive elements. The results (Fig. 7) show that both models predict high shear stresses on either side of the ends of the defect, but also that the failure patterns are different. In columnar nacre the deformation localized along a band perpendicular to the loading direction, following a columnar type of failure. In contrast, sheet nacre showed two localizations at an angle, triggered in the regions of high shear stresses and thus following a stair type of failure. These models clearly show that (i) a combination of shear and microstructure can trigger stair failure and (ii) stair failure enables the spreading of inelastic deformation over large volumes, even in the absence of any source of hardening.

4.2. Microstructures with statistics

Finally, more realistic RVE models were generated using statistics (normal distributions) for tablet thickness, length and waviness. The random waviness of the tablet contours was created using piecewise half-sine functions. The amplitude, wavelength and phase of each half-sine function was generated from a normal distribution then positioned end to end. The statistical parameters were adjusted to match actual nacreous microstructure [10]. A “columnar” model was generated, where the arrangement and overlap of the tablets were chosen to duplicate the actual structure of columnar nacre (Fig. 8a). A “sheet” model was also constructed based on the exact same tablets statistics, except that the tablets were arranged randomly from one layer to the next (Fig. 8b). The overall size of the RVE was chosen so that the results were not RVE size dependant (i.e. the RVE was large enough for the statistics used).

The resulting RVE stress–strain curves are shown in Fig. 9. Experimental observations were duplicated, with tablet sliding generating inelastic strains. This process was accompanied by hardening generated by the waviness of the tablets. Interestingly, hardening, well documented for columnar nacre [10], was also observed in sheet nacre, even in the absence of well-defined core and overlap regions.

The displacement contours along the loading direction (Fig. 8a) show that the columnar model develops relatively uniform distribution of deformation bands throughout the RVE. The overlap regions provide “predefined” locations for deformation bands, perpendicular to the loading direction. The hardening generated by the waviness of the tablets produces new deformation bands until saturation of the model. In contrast, the deformation bands in the sheet model appeared in stair patterns (Fig. 8b). A large number of junctions remained closed (Fig. 8c), which is also consistent with the experimental observations. The stair deformation bands eventually coalesced and formed jagged deformation bands across the loading direction. Some hardening mechanism caused these jagged deformation bands to multiply and spread, forming

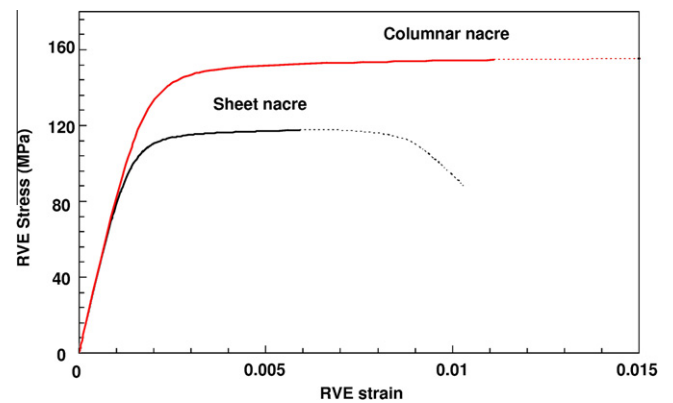


Fig. 9. Stress–strain curves for the columnar and sheet models with statistics (dotted lines correspond to deformation with no strain hardening).

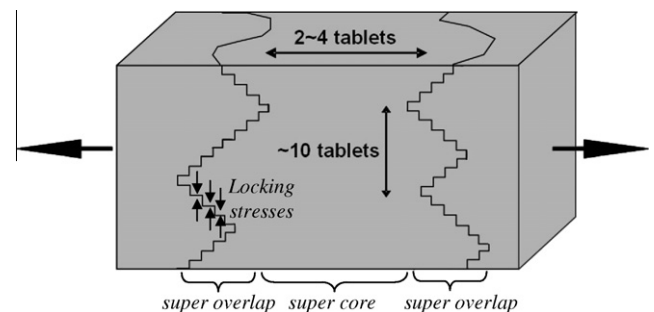


Fig. 10. Proposed deformation pattern for sheet nacre. Stair failures coalesce and form “super columns” and “super cores”, favorable to the build-up of transverse stresses and hardening.

a structure made of “super core” and “super overlap” regions of several tablets in length (Fig. 10). Note that even though the RVE was loaded in uniaxial tension, local shear stresses are in this case generated by inhomogeneities in the model.

Interestingly, the hardening mechanisms in sheet nacre were also captured in this model. The wavy tablets also generated progressive locking, but in sheet nacre the transverse compression built up occurred in “super overlap” regions several tablets long, which was balanced by transverse tension in “super core” regions (Fig. 10). The hardening mechanism is the same for both columnar and sheet naces, but in sheet nacre it operates on a larger length scale.

5. Conclusions

Nacre, one of the most remarkable hard natural materials known, is increasingly serving as a model for the design of biomimetic materials. In this context, this work provides new insights into the construction and mechanics of this material.

- All naces are not equal in performance and mechanisms: within the four naces tested in this study, sheet nacre from the pearl oyster was significantly superior in toughness, and should probably serve as a model for future biomimetic materials.
- Sheet nacre from the pen shell performed relatively poorly (Fig. 1). The low fracture toughness of the pen shell may be attributed to its higher tablet aspect ratio (Table 2), to large variations in waviness and to growth defects. These features may raise the stresses in the tablets significantly, which may

lead to premature fracture of the tablets before they can actually slide on one another. The toughness of nacre relies on molecular events at the interface of the tablets [6]. Possible deficiencies in the organic materials of the pen shell could therefore also explain its lower fracture toughness.

- For all nacres tested the toughness correlated well with the size of the process zone around the crack, which strongly suggests that the process zone is a prominent toughening mechanism in nacre. This corroborates previous studies on red abalone nacre [11].
- While columnar nacre developed well-defined deformation bands following the columnar structure and perpendicular to the loading direction, sheet nacre from the pearl oyster developed a quite unusual network of deformation bands at an angle to the main crack. Analytical and numerical models demonstrated that the transition between columnar and stair failure modes is controlled by the amount of overlap between tablets and by local shear stresses due to inhomogeneities in the material. Stair failure was shown to lower the tensile strength of the material, which may be compensated for by the longer overlap length in microstructures favorable to this type of failure.
- In terms of toughness enhancement the stair deformation mode appears to be more beneficial than columnar deformation, because it can spread over a large volume even in the absence of any hardening mechanism (thereby promoting energy dissipation and toughening).
- The jagged deformation bands in sheet nacre develop and spread with several tablets spacing, forming “super core” and “super overlap” regions. These regions are favorable to the development of tablet waviness-based hardening in the material.

Finally, these new findings on sheet nacre and stair failure may be generalized to other natural composites with a random staggered arrangement. In particular, the conditions for the stair failure mode are met in bone on the microscale. Mineralized collagen fibrils are aligned with a random overlap and the “ductility” of bone in tension is provided by the sliding of those fibrils along one another [15]. The models developed so far to capture this fundamental mechanism have assumed a columnar type of failure, whereas a stair type of failure may actually prevail in this case, with important implications for the strength and toughness of bone on the smallest scales.

Acknowledgements

This work was supported by the Faculty of Engineering at McGill University, the Natural Sciences and Engineering Research Council of Canada, the Canada Foundation for Innovation and the Fonds Québécois de la Recherche sur la Nature et les Technologies. The first pearl oyster samples were generously provided by Evelyne Lopez from the Musée National d'Histoire Naturelle in Paris, France.

Appendix A. Details of the analytical model

Fig. A1 shows the representative volume element (RVE) used to develop the analytical model. The RVE is similar to models proposed previously [16,17], but here the overlap between tablet can be less than half of the tablet length, and in addition a shear stress is superimposed on the tensile stress. The junctions (vertical interfaces) between the tablets are ignored (their only effect is to increase the modulus and strength without affecting the mechanics of deformation).

Let τ_{O_1} , τ_{O_2} be the average shear stresses at the overlap regions and τ_{C_1} , τ_{C_2} the average shear stresses at the core regions (Fig. A1).

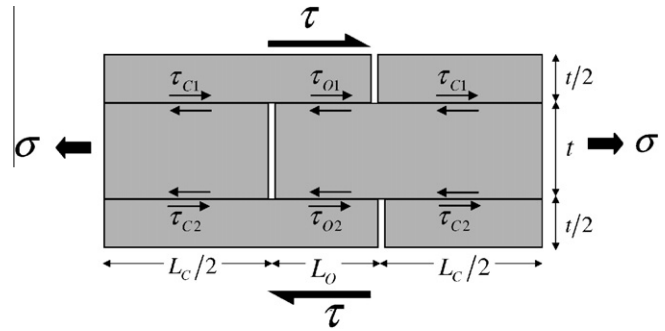


Fig. A1. Schematic of a RVE subjected to tension and shear. Shear stresses transmitted through the overlap (τ_{O_1} , τ_{O_2}) and core regions (τ_{C_1} , τ_{C_2}) are also shown.

Examination of the load transfer at the interfaces and equilibrium equations leads to the three independent equations:

$$\begin{aligned} (1 - \beta)\tau_{C_1} + \beta\tau_{O_1} &= \tau \\ (1 - \beta)\tau_{C_2} + \beta\tau_{O_2} &= \tau \\ \alpha(\tau_{O_2} - \tau_{O_1}) &= 2\sigma \end{aligned} \quad (1)$$

where $\alpha = L_o/t$ and $\beta = L_c/L$. This forms a system of three equations for four unknowns. In the linear range the shear stresses can, however, be found using additional relations from superimposition and symmetries, leading to the solution:

$$\begin{aligned} \tau_{O_1} &= \tau - (\sigma/\alpha) \\ \tau_{O_2} &= \tau + (\sigma/\alpha) \\ \tau_{C_1} &= \tau + (\beta/1 - \beta)(\sigma/\alpha) \\ \tau_{C_2} &= \tau - (\beta/1 - \beta)(\sigma/\alpha) \end{aligned} \quad (2)$$

where σ and τ are the applied tensile and shear stresses. Note that these shear stresses result from the applied shear and by the tensile load transfer mechanism.

Now let τ_s be the shear strength of the interface. If $\tau > 0$ and $\beta < 1$, the first interface to fail will be at overlap O_2 , and upon failure $\tau_{O_2} = \tau_s$. If the applied stresses are increased further the stresses will be redistributed and symmetries will be lost. However the remaining shear stresses can now be found using (1). The solutions, normalized by τ_s , are:

$$\begin{aligned} (\tau_{O_1}/\tau_s) &= \tau_{O_1}^* = 1 - 2\sigma^* \\ (\tau_{O_2}/\tau_s) &= \tau_{O_2}^* = 1 \\ (\tau_{C_1}/\tau_s) &= \tau_{C_1}^* = [\tau^* - \beta(1 - 2\sigma^*)]/(1 - \beta) \\ (\tau_{C_2}/\tau_s) &= \tau_{C_2}^* = (\tau^* - \beta)/(1 - \beta) \end{aligned} \quad (3)$$

where $\tau^* = \tau/\tau_s$ and $\sigma^* = \sigma/\alpha\tau_s$. Regions C_2 , O_1 or C_1 may fail next and trigger one of three failure modes. In the first case, C_2 will fail next if $\tau^* = 1$, regardless of the applied tensile stress. This corresponds to a “shearing” type of failure. For the second case where $0 < \tau^* < 1 - 2\beta$, overlap region O_1 will fail after O_2 , generating a “columnar” type of failure with deformation bands perpendicular to the loading direction. For the third case where $1 - 2\beta < \tau^* < 1$, core region C_1 will fail after O_2 , generating a “stair” type of failure where deformation bands are at an angle to the loading direction.

Appendix B. Figures with essential colour discrimination

Certain figures in this article, particularly Figures 1–4, 6–9 and Table 1, are difficult to interpret in black and white. The full colour images can be found in the on-line version, at doi:10.1016/j.actbio.2010.04.008.

References

- [1] Wegst UGK, Ashby MF. The mechanical efficiency of natural materials. *Philos Mag* 2004;84:2167.
- [2] Barthelat F. Biomimetics for next generation materials. *Philos Trans R Soc A Math Phys Eng Sci* 2007;365:2907.
- [3] Currey JD. Mechanical properties of mother of pearl in tension. *Proc R Soc Lond* 1977;196:443.
- [4] Bonderer LJ, Studart AR, Gauckler LJ. Bioinspired design and assembly of platelet reinforced polymer films. *Science* 2008;319:1069.
- [5] Munch E, Launey ME, Alsem DH, Saiz E, Tomsia AP, Ritchie RO. Tough, bio-inspired hybrid materials. *Science* 2008;322:1516.
- [6] Smith BL, Schaeffer TE, Viani M, Thompson JB, Frederick NA, Kindt J, et al. *Nature* (London) 1999;399:761.
- [7] Lin AYM, Meyers MA. Interfacial shear strength in abalone nacre. *J Mech Behav Biomed Mater* 2009;2:607.
- [8] Wang RZ, Suo Z, Evans AG, Yao N, Aksay IA. Deformation mechanisms in nacre. *J Mater Res* 2001;16:2485.
- [9] Song F, Bai YL. Effects of nanostructures on the fracture strength of the interfaces in nacre. *J Mater Res* 2003;18:1741.
- [10] Barthelat F, Tang H, Zavattieri PD, Li CM, Espinosa HD. On the mechanics of mother-of-pearl: a key feature in the material hierarchical structure. *J Mech Phys Solids* 2007;55:225.
- [11] Barthelat F, Espinosa HD. An experimental investigation of deformation and fracture of nacre-mother of pearl. *Exp Mech* 2007;47:311.
- [12] Jackson AP, Vincent JFV, Turner RM. The mechanical design of nacre. *Proc R Soc Lond* 1988;234:415.
- [13] Deville S, Saiz E, Nalla RK, Tomsia AP. Freezing as a path to build complex composites. *Science* 2006;311:515.
- [14] Gao HJ. Application of fracture mechanics concepts to hierarchical biomechanics of bone and bone-like materials. *Int J Fract* 2006;138:101.
- [15] Gupta HS, Seto J, Wagermaier W, Zaslansky P, Boesecke P, Fratzl P. Cooperative deformation of mineral and collagen in bone at the nanoscale. *Proc Natl Acad Sci USA* 2006;103:17741.
- [16] Jager I, Fratzl P. Mineralized collagen fibrils: a mechanical model with a staggered arrangement of mineral particles. *Biophys J* 2000;79:1737.
- [17] Kotha SP, Li Y, Guzelsu N. Micromechanical model of nacre tested in tension. *J Mater Sci* 2001;36:2001.
- [18] ASTM. Standard test method for measurement of fracture toughness, ASTM Standard E 1820-01. West Conshohocken, PA: ASTM International; 2004.
- [19] Saxena A. Nonlinear fracture mechanics. Boca Raton, FL: CRC Press; 1998.
- [20] Sakai M, Bradt RC. Fracture-toughness testing of brittle materials. *Int Mater Rev* 1993;38:53.
- [21] Menig R, Meyers MH, Meyers MA, Vecchio KS. Quasi-static and dynamic mechanical response of *Haliotis rufescens* (abalone) shells. *Acta Mater* 2000;48.
- [22] Bruet BFF, Qi HJ, Boyce MC, Panas R, Tai K, Frick L, et al. Nanoscale morphology and indentation of individual nacre tablets from the gastropod mollusc *Trochus niloticus*. *J Mater Res* 2005;20:2400.
- [23] Barthelat F, Li CM, Comi C, Espinosa HD. Mechanical properties of nacre constituents and their impact on mechanical performance. *J Mater Res* 2006;21:1977.